# In vivo fluorescence lifetime tomography of a FRET probe expressed in mouse

**James McGinty,[1,5] Daniel W. Stuckey,[2,5] Vadim Y. Soloviev,[3] Romain Laine,[1] Marzena Wylezinska-Arridge,[2] Dominic J. Wells,[4] Simon R. Arridge,[3] Paul M. W. French,[1] Joseph V. Hajnal,[2] and Alessandro Sardini[2,*]**

*[1]Photonics Group, Blackett Laboratory, Imperial College London, London SW7 2BW, UK*
*[2]MRC Clinical Sciences Centre, Imperial College London, Hammersmith Hospital Campus, London W12 0NN, UK*
*[3]Department of Computer Science, University College London, London WC1E 6BT, UK*
*[4]Department of Veterinary Basic Sciences, The Royal Veterinary College, London NW1 0TU, UK*
*[5]These authors contributed equally to this work*
**a.sardini@csc.mrc.ac.uk*

**Abstract:** Förster resonance energy transfer (FRET) is a powerful biological tool for reading out cell signaling processes. *In vivo* use of FRET is challenging because of the scattering properties of bulk tissue. By combining diffuse fluorescence tomography with fluorescence lifetime imaging (FLIM), implemented using wide-field time-gated detection of fluorescence excited by ultrashort laser pulses in a tomographic imaging system and applying inverse scattering algorithms, we can reconstruct the three dimensional spatial localization of fluorescence quantum efficiency and lifetime. We demonstrate *in vivo* spatial mapping of FRET between genetically expressed fluorescent proteins in live mice read out using FLIM. Following transfection by electroporation, mouse hind leg muscles were imaged *in vivo* and the emission of free donor (eGFP) in the presence of free acceptor (mCherry) could be clearly distinguished from the fluorescence of the donor when directly linked to the acceptor in a tandem (eGFP-mCherry) FRET construct.



**OCIS codes:** (170.2655) Functional monitoring and imaging; (170.3010) Image reconstruction techniques; (170.3650) Lifetime-based sensing; (170.3660) Light propagation in tissues; (170.3880) Medical and biological imaging; (170.6960) Tomography.

## References and links

1. S. S. Vogel, C. Thaler, and S. V. Koushik, "Fanciful FRET," Sci. STKE **2006**(331), re2 (2006).
2. E. A. Jares-Erijman and T. M. Jovin, "Imaging molecular interactions in living cells by FRET microscopy," Curr. Opin. Chem. Biol. **10**(5), 409–416 (2006).
3. V. Ntziachristos, "Fluorescence molecular imaging," Annu. Rev. Biomed. Eng. **8**(1), 1–33 (2006).
4. J. R. Lakowicz, *Principles of Fluorescence Spectroscopy* (Springer, NY, 2006).
5. J. C. Hebden, S. R. Arridge, and D. T. Delpy, "Optical imaging in medicine: I. Experimental techniques," Phys. Med. Biol. **42**(5), 825–840 (1997).
6. J. McGinty, V. Y. Soloviev, K. B. Tahir, R. Laine, D. W. Stuckey, J. V. Hajnal, A. Sardini, P. M. French, and S. R. Arridge, "Three-dimensional imaging of Förster resonance energy transfer in heterogeneous turbid media by tomographic fluorescent lifetime imaging," Opt. Lett. **34**(18), 2772–2774 (2009).
7. R. E. Nothdurft, S. V. Patwardhan, W. Akers, Y. Ye, S. Achilefu, and J. P. Culver, "*In vivo* fluorescence lifetime tomography," J. Biomed. Opt. **14**(2), 024004 (2009).
8. A. L. Rusanov, T. V. Ivashina, L. M. Vinokurov, I. I. Fiks II, A. G. Orlova, I. V. Turchin, I. G. Meerovich, V. V. Zherdeva, and A. P. Savitsky, "Lifetime imaging of FRET between red fluorescent proteins," J Biophotonics **3**(12), 774–783 (2010).
9. V. Gaind, S. Kularatne, P. S. Low, and K. J. Webb, "Deep-tissue imaging of intramolecular fluorescence resonance energy-transfer parameters," Opt. Lett. **35**(9), 1314–1316 (2010).
10. V. Y. Soloviev, J. McGinty, K. B. Tahir, R. Laine, D. W. Stuckey, P. S. Mohan, J. V. Hajnal, A. Sardini, P. M. W. French, and S. R. Arridge, "Tomographic imaging of fluorescence resonance energy transfer in highly light scattering media," Proc. SPIE **7573**, 75730G, 75730G-10 (2010).
11. J. M. McMahon, E. Signori, K. E. Wells, V. M. Fazio, and D. J. Wells, "Optimisation of electrotransfer of plasmid into skeletal muscle by pretreatment with hyaluronidase—increased expression with reduced muscle damage," Gene Ther. **8**(16), 1264–1270 (2001).

#146182 - $15.00 USD Received 18 Apr 2011; revised 6 Jun 2011; accepted 10 Jun 2011; published 10 Jun 2011

12. O. Boussif, F. Lezoualc'h, M. A. Zanta, M. D. Mergny, D. Scherman, B. Demeneix, and J. P. Behr, "A versatile vector for gene and oligonucleotide transfer into cells in culture and *in vivo*: polyethylenimine," Proc. Natl. Acad. Sci. U.S.A. **92**(16), 7297–7301 (1995).
13. H. B. Manning, G. T. Kennedy, D. M. Owen, D. M. Grant, A. I. Magee, M. A. Neil, Y. Itoh, C. Dunsby, and P. M. French, "A compact, multidimensional spectrofluorometer exploiting supercontinuum generation," J Biophotonics **1**(6), 494–505 (2008).
14. V. Y. Soloviev, C. D'Andrea, P. S. Mohan, G. Valentini, R. Cubeddu, and S. R. Arridge, "Fluorescence lifetime optical tomography with Discontinuous Galerkin discretisation scheme," Biomed. Opt. Express **1**(3), 998–1013 (2010).
15. V. V. Sobolev, *A Treatise on Radiative Transfer* (D. Van Nostrand, Princeton, 1963).
16. J. Nocedal and S. J. Wright, *Numerical Optimization* (Springer-Verlag, New York, 1999).
17. C. I. Maeder, M. A. Hink, A. Kinkhabwala, R. Mayr, P. I. Bastiaens, and M. Knop, "Spatial regulation of Fus3 MAP kinase activity through a reaction-diffusion mechanism in yeast pheromone signalling," Nat. Cell Biol. **9**(11), 1319–1326 (2007).
18. N. C. Deliolanis, T. Wurdinger, L. Pike, B. A. Tannous, X. O. Breakefield, R. Weissleder, and V. Ntziachristos, "*In vivo* tomographic imaging of red-shifted fluorescent proteins," Biomed. Opt. Express **2**(4), 887–900 (2011).
19. S. B. VanEngelenburg and A. E. Palmer, "Fluorescent biosensors of protein function," Curr. Opin. Chem. Biol. **12**(1), 60–65 (2008).
20. B. Ananthanarayanan, Q. Ni, and J. Zhang, "Chapter 2: Molecular sensors based on fluorescence resonance energy transfer to visualize cellular dynamics," Methods Cell Biol. **89**, 37–57 (2008).

## 1. Introduction

The combination of genetically encoded fluorescent proteins and Förster resonance energy transfer (FRET) has become an important tool for reading out cell signaling processes [1,2] and a significant arsenal of FRET probes has been developed. To date, such readouts have been largely confined to fluorescence microscopy of cells in culture. It is becoming increasingly important to translate FRET assays to small animal imaging where the *in vivo* physiological context is important for drug development, the study of diseases and fundamental cellular and molecular biology [3].

FRET is the radiationless transfer of energy from an excited donor fluorophore to an appropriate acceptor in close proximity and is accompanied by a reduction of the donor fluorescence lifetime and quantum yield. Because fluorescence lifetime measurements are inherently ratiometric and therefore relatively insensitive to variations in fluorophore concentration, optical scattering and detection efficiency [4], FLIM provides one of the most robust quantitative methods for mapping FRET.

We are developing a tomographic imaging capability for small animals that utilizes FLIM to read out and localize FRET, which we have demonstrated by applying it to live mice transfected with genetically expressed fluorophores. The ability to localize and quantitatively reconstruct fluorescence parameters in biological tissues is limited by absorption and by the diffusive nature of light transport in such highly scattering media. Diffuse imaging and tomography has been extensively investigated in brain and breast tissue, achieving ~cm spatial precision using near infra-red radiation [5] but optical scattering and absorption preclude imaging with visible radiation with such large samples. However, the smaller length scale (sub-cm) associated with murine tomography can permit the use of shorter wavelength (visible) emitting fluorophores, including genetically expressed labels such as eGFP, and allows such fluorophores to be mapped with greater spatial precision. When imaging mice, the diffuse nature of light transport still presents a significant challenge for accurate optical measurements. However, the instrumentation for time-resolved detection that is required to determine fluorescence lifetimes also provides a means to characterize diffuse light transport and, by employing a time-resolved model for diffuse optical tomography, we are able to reconstruct three dimensional maps of fluorescence lifetime and quantum yield, as well as the optical properties of the sample [6].

We note that, although FLIM and FRET are well established for cell microscopy, FLIM has only recently been demonstrated in live mouse models, implemented with tomography to image dye phantoms and subcutaneous tumors targeted with a fluorescent marker [7] or expressing a fluorescent protein [8]. To date, intensity-based FRET tomography [9] and FLIM FRET have only been applied to mice *ex vivo* [8]. We report here a tomographic approach to monitor *in vivo* FLIM FRET readouts and demonstrate for the first time the reconstruction of

#146182 - $15.00 USD Received 18 Apr 2011; revised 6 Jun 2011; accepted 10 Jun 2011; published 10 Jun 2011

the lifetime and quantum yield of a genetically expressed FRET probe measured *in vivo*. This non-invasive approach can facilitate the *in vivo* localization of appropriate FRET probes for biomedical research and drug discovery, permitting longitudinal studies with a reduced number of animals.

## 2. Materials and methods

### *2.1. Experimental setup and acquisition conditions*

Using the experimental setup illustrated in Fig. 1, we applied FLIM to read out FRET in live mice expressing GCLink, a FRET construct in which eGFP (donor) is directly coupled by a short flexible linker to mCherry (acceptor). Plasmids were transfected by electroporation into the right hind leg. This procedure primarily targets the tibialis anterior (TA) muscle although it does label some of the surrounding muscles in the anterior lateral quadrant of the leg. Control mice were co-transfected with plasmids separately coding for eGFP and mCherry to co-express the free donor and acceptor fluorophores. At the peak of GCLink expression (5 or 6 days after transfection) the mice were anaesthetized and positioned on a rotating imaging platform such that their legs could be tomographically imaged in a transmission geometry (Fig. 1, panel b). eGFP was excited using ultrashort (~10 ps) pulses of radiation at 480 nm (40 nm spectral width) from a spectrally filtered ultrafast supercontinuum laser source that was focused on the surface of the mouse leg. The laser beam incident at the sample was typically of 10 mW average power and illuminated an area of 0.2 $mm^2$, corresponding to an intensity of 5 $Wcm^{-2}$. The exposure time varied from mouse to mouse depending on the expression level of the eGFP and the attenuation of its fluorescence. Total image acquisition times per mouse varied from 492 s to 2364 s with an average of 1112 s. The transmitted excitation light and the emitted fluorescence were imaged onto a time-gated optical intensifier (GOI) and sequentially read out using a charge couple device (CCD) camera (Fig. 1, panel a).

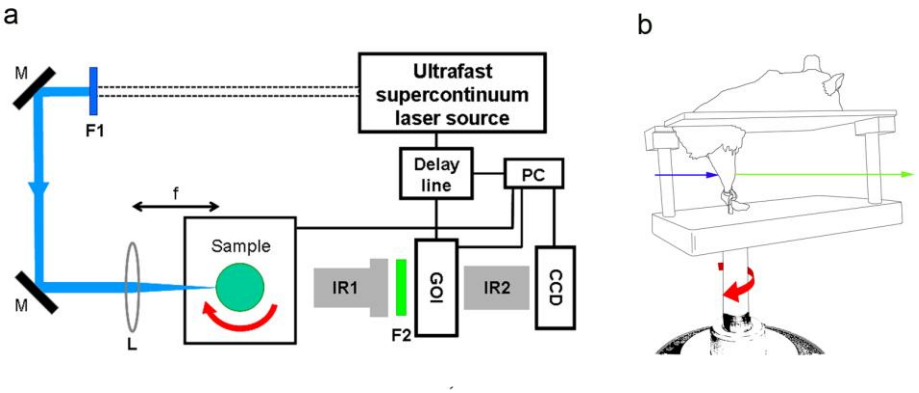


Fig. 1. Schematic of the *in vivo* time-gated imaging setup. (a) Ultrashort pulses of radiation from a spectrally filtered supercontinuum laser were focused on the surface of the mouse leg. The emerging fluorescence light distribution was imaged onto the GOI and read out using the CCD. (b) The anaesthetized mouse was positioned on the imaging platform, which was set on a motorised rotation stage controlled by the PC. The target leg was held under slight tension by an elastic band. M, Mirror; F1, Filter 1; F2, Filter 2; L, Lens; IR1, Image Relay 1; IR2, Image Relay 2; GOI, Gated-Optical Intensifier; CCD, Charged-Couple Device camera; PC, Personal Computer.

Wide-field time-gated images were acquired at each of 12 angular orientations. For efficient computation, the time-resolved tomographic fluorescence image stacks were Fourier transformed to the frequency domain and the 3-D fluorescence lifetime distribution was reconstructed under the assumption of a mono-exponential fluorescence decay profile using an inverse scattering algorithm based on a variational framework [10]. Besides the fluorescence lifetime, this algorithm also reconstructed the 3-D distribution of fluorophore quantum yield (defined as the ratio of the emitted fluorescence energy to the absorbed

#146182 - $15.00 USD Received 18 Apr 2011; revised 6 Jun 2011; accepted 10 Jun 2011; published 10 Jun 2011

excitation energy per voxel) and the scattering and absorption coefficients. Details of the individual component parts of this procedure follow together with the anatomical/structural imaging techniques that were used to verify the localization of the signals obtained.

### *2.2. DNA plasmids*

Standard splicing PCR was used to generate the fused expression construct GCLink. In brief, full-length open reading frames of enhanced Green Fluorescent Protein (pEGFP-C1 vector, Clontech) and mCherry (pmCherry-C1 vector, Clontech) were amplified with an overlapping region consisting of a glycine-glycine-serine-glycine-glycine-serine linker. The two gel purified products were mixed and a second PCR initiated with oligos allowing amplification of a fused construct. The fused PCR product was gel purified and cloned into pTriEx4 (Novagen). Cloned constructs were verified by sequencing.

### *2.3. In vivo plasmid electroporation*

Plasmid DNA was transformed into JM109 bacteria (Promega) and purified using EndoFree plasmid kits (Qiagen). DNA was ethanol precipitated and resuspended in phosphate buffered saline, pH 7.4 (Invitrogen) to a concentration of 1 μg/μl (GCLink) or 1.5 μg/μl (individual eGFP and mCherry fluorophores).

*In vivo* experiments were conducted on 6- to 8-week old CD1 female mice. Animals were housed in a minimal disease facility with *ad libitum* food and water. Animals were placed under general anaesthetic by peritoneal injection of the following mixture: one part fentanyl/fluanisone (Hypnorm, Janssen Animal Health), one part midazolam (Roche), two parts distilled water at 10 ml/kg. TA muscles were pretreated by injecting 0.4 U/μl bovine hyaluronidase (H-4272, Sigma) in 25 μl normal saline, 1 hr before plasmid injection. Plasmid DNA was injected percutaneously in a proximal to distal direction inside the TA muscle. A total of 25 μg plasmid DNA was injected into the muscle using a 1 ml insulin syringe with an integrated 29G needle. Following the intramuscular injection of plasmid DNA an electric field was applied to the muscle as previously described [11]. The injected leg was held steady and 7 mm circular electrodes (Tweezertrodes, Harvard Apparatus) were applied to the medial and lateral sides of the lower hind limb. An electric field of 175 V/cm was applied in 20 ms square wave pulses 10 times at 1 second intervals using a BTX ECM 830 electroporator. Optical acquisition took place 5 or 6 days after the injection of plasmid DNA, at the height of protein expression.

### *2.4. In vivo imaging*

All animal experiments were carried out under license from the Home Office (UK) in accordance with The Animal (Scientific Procedure) Act 1986 and Imperial College London guidelines.

General anesthesia was induced in mice as described above and maintained by *i.p.* injection of 0.3 ml/kg fentanyl/fluanisone when necessary. Body temperature was monitored and maintained using a jet of warm air. Vital parameters such as heart beat frequency and blood oxygenation were monitored using a pulse oximeter (STARR). Hair was chemically removed from the electroporated leg using depilatory cream.

Anaesthetized mice were positioned in a custom-built platform on a rotation stage (URS75CC, Newport Corp) with the target leg held under tension by an elastic band so that it remained approximately aligned with the axis of rotation. The filtered pulsed supercontinuum source (SC400-2, Fianium Ltd) was focused to ~0.5mm spot on the surface of the leg. The excitation and fluorescence light transmitted through the leg was imaged at 480nm and 530 nm respectively each with a 40nm bandwidth. Sequential acquisitions were obtained with the time-gated optical intensifier (HRI, Kentech Instruments Ltd) read out by the CCD camera (ORCA, Hamamatsu Photonics UK Ltd). The intensifier's gate-width was set to 1 ns and the excitation and fluorescence light was sampled over a 10 ns window at 250 ps intervals such that the growth and decay of the optical signals were acquired. Synchronization was achieved using a photodiode trace from the excitation source as a trigger signal for the HRI via a

#146182 - $15.00 USD Received 18 Apr 2011; revised 6 Jun 2011; accepted 10 Jun 2011; published 10 Jun 2011

computer controlled electronic delay line (Precision Delay Generator, Kentech Instruments Ltd). This acquisition procedure was repeated at 12 angular orientations collected (~30° separation) with the lateral spot position centered to within 1mm for each orientation. The geometrical positions of the excitation spots were measured separately at the end of each experiment so that the source position is known for each image set. In addition, silhouette images (shadowgrams) were acquired at 1° rotation steps over a complete revolution and used to extract the surface of the mouse leg using a filtered back-projection algorithm.

*2.5. MRI acquisition*

Following optical acquisition the mouse was euthanized by terminal anesthetic overdose. To maintain its pose the leg was embedded in 1% agarose (Sigma). When the agarose had solidified, the leg was cut away from the rest of the body at the level of the hip. The embedded leg was then imaged at 9.4 T (Varian Inc) in a 35 mm birdcage transmit-receiver coil (Rapid Biomedical) using a multi-slice T1 weighted spin echo acquisition (TR = 500 ms, TE = 8.74 ms) acquired transverse to the leg with a slice thickness of 0.5 mm and 59 μm x 59 μm in-plane resolution.

*2.6. Confocal fluorescence microscopy and whole leg histology*

Electroporated legs were excised *post mortem* and the TA muscles removed, mounted on a cork block, embedded in O.C.T. compound (BDH Laboratory Supplies) and snap-frozen in liquid nitrogen-cooled isopentane. Samples were stored at −80°C. To verify transfection, frozen muscles and whole legs were sliced using a cryostat. Transverse sections were cut at a thickness of 80 μm and lifted onto poly-L-lysine-coated slides (VWR). Cryosections were fixed in 4% formaldehyde with 4% sucrose for 20 minutes at room temperature, washed in PBS and mounted in Vectashield (Vectorlabs). Confocal fluorescence images were acquired on a Leica TCS SP5 confocal microscope with a HC PL APO 20x/0.70NA objective lens. eGFP was excited at 488 nm and detected at 499-540 nm, while mCherry was excited at 561 nm and detected at 600-684 nm. Transverse leg sections were acquired using an Olympus SZX16 fluorescence microscope with an SDFPLAPO 0.5x parfocal objective lens and appropriate filters to observe eGFP and mCherry.

*2.7. Spectroscopy analysis*

Plasmid DNA was transiently transfected into HEK293T cells using a standard PEI transfection protocol [12]. Transfected cells were homogenized in ice cold lysis buffer: 50 mM mannitol, 2 mM EDTA, 50 mM Tris HCl, pH 7.4 with complete protease inhibitors (Roche). Nuclei and debris were pelleted by centrifugation at 500 g for 10 min at 4°C, and the supernatant was loaded onto a cushion of 300 mM mannitol, 50 mM Tris-HCl, pH 7.6 and complete protease inhibitors. The total membrane fraction was pelleted by centrifugation at 40,000 g for 45 min at 4°C, and the supernatant was collected as a cytosol preparation and stored at −80°C.

Fluorescence lifetime cuvette measurements were performed with an in-house built time-resolved spectrofluorometer [13] that incorporates a tunable supercontinuum excitation source (SPC-400, Fianium Ltd). eGFP was excited at 488 nm using a 10 nm bandpass filter and emission was collected at 510 nm via a 10 nm bandpass filter. Time-resolved detection was implemented using time-correlated single photon counting (TCSPC) with a photomultiplier tube (PMC-100, Becker & Hickl GmbH, Berlin, Germany) connected to TCSPC electronics (SPC-730, Becker & Hickl GmbH). To analyze the fluorescence data, the instrument response function (IRF) was acquired at the excitation wavelength using a colloidal silica suspension (LUDOX® SM-30, Aldrich Chemical Company Inc.) and included in the fitting model. All fluorescence lifetime measurements were carried out by exciting the sample with a vertical polarization and measuring its emission at the magic angle polarization.

Lifetime data analysis of eGFP was conducted by using a double exponential decay model, see Eq. (1) below, convolved with the IRF.

#146182 - $15.00 USD Received 18 Apr 2011; revised 6 Jun 2011; accepted 10 Jun 2011; published 10 Jun 2011

$$I(t) = p_1 e^{-\frac{t}{\tau_1}} + p_2 e^{-\frac{t}{\tau_2}} \quad (1)$$

Fitting of the experimental data was performed with TRFA Data Processor Advanced (SSTC, Minsk, Belarus). The average lifetime ( $\bar{\tau}$ ) was calculated following Eq. (2):

$$\bar{\tau} = \frac{p_1\tau_1^2 + p_2\tau_2^2}{p_1\tau_1 + p_2\tau_2} \quad (2)$$

*2.8. Tomographic reconstruction*

Tomographic "image" reconstruction was based on the principle of implementing a numerical model of diffuse light propagation (the forward model) and fitting this model to the measured data (inverse problem). This inverse scattering approach provides the most probable (in the *a posteriori* sense) three dimensional distribution of optical and fluorescence parameters to have produced the experimentally measured data, known as the *Maximum A Posteriori* (MAP) estimate. In general, this is an ill-posed problem and the resulting reconstructions should be considered as statistical indications of fluorophore distributions rather than conventional images that have a direct voxel by voxel correspondence to the sample.

The model of light propagation in the time domain, where the measurements are taken, is given by the Telegraph equation approximation to the Radiative Transfer Equation; for more details see reference [14]. To solve the equations more efficiently, we first convert the measured data into the frequency domain by fast Fourier transform (FFT) and then use the Helmholtz equation for the light model (the Fourier equivalent of the Telegraph model) at multiple harmonic samples that can be solved in parallel. The model was implemented on a Cartesian grid by utilizing the Finite Volume numerical scheme. The computational domain is split into computational cells (voxels), whose dimensions correspond to the pixel dimensions in the CCD array. The computational mesh was built using a filtered back projection of shadowgrams of the mouse's leg, acquired at 1° angular steps. The total number of computational voxels varied from 300,000 to 500,000 depending on leg's size.

In addition to modeling light propagation inside the leg, a method is required for mapping the experimentally recorded time-gated "images" onto the surface of the scattering object. This mapping is performed by converting the intensity recorded by the CCD camera to the energy density by taking into account an angular dependence of radiation leaving the surface. For this purpose we employ the method of Schwarzschild-Shuster [15], which results in an image brightness correction factor $(½ + \cos\theta)^{-1}$, where $\theta$ is the angle between surface normal and direction to the CCD camera.

Model fitting for the inverse problem is based on minimization of an error functional representing the squared difference between the measured and modeled data for both excitation and fluorescence. Because the inverse problem is strongly ill-posed, the error functional is augmented by a regularization functional [10,15]. The minimization is carried out by a nonlinear conjugate gradient (NLCG) algorithm constrained by the solution of the forward problem. The functional gradient used in the NLCG algorithm is computed using the solution of the forward problem and a corresponding adjoint problem for each position of the laser source. The solution of the adjoint problem uses the same computational grid as the forward problem applied in reverse to calculate the light distribution solved using the CCD array as a source. The resulting system represents the Karush-Kuhn-Tucker conditions [16] for optimization of the error norm with the given light transport model. Since an iteration of the forward problem requires the solution of four Helmholtz equations for excitation, fluorescent and two corresponding adjoint energy densities, computation of optical and fluorescence parameters may take up to 7 minutes for each projection angle on a 2.16 GHz processor. In total, reconstruction takes up to 2 hours for 12 projection angles at one frequency.

#146182 - $15.00 USD Received 18 Apr 2011; revised 6 Jun 2011; accepted 10 Jun 2011; published 10 Jun 2011

## 3. Results and discussion

Figure 2 shows cross sections from tomographic reconstructions of the eGFP donor fluorescence lifetime distributions from imaging the hind legs in two live transfected mice. Panel (a) corresponds to a leg containing muscles expressing the FRET construct, GCLink, whilst panel (b) displays the non-FRETing control co-expressing eGFP and mCherry separately and panel (c) shows the corresponding lifetime histograms for both.

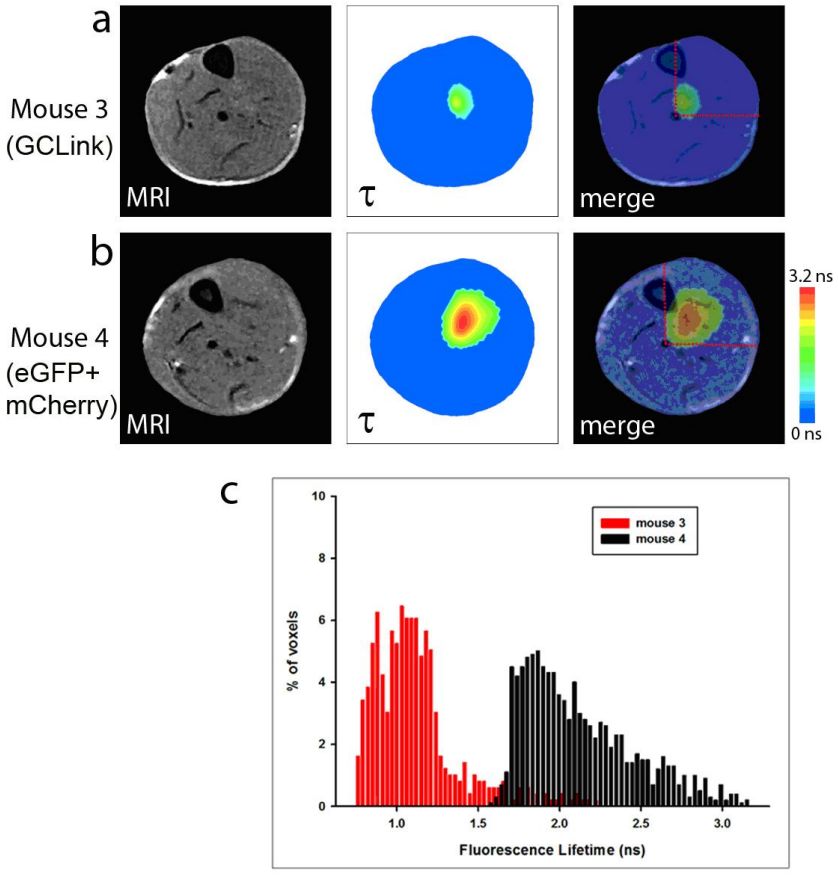


Fig. 2. Transverse sections from tomographic reconstructions of MRI and fluorescence lifetime from *in vivo* measurements of mouse hind legs. Panels show leg cross sections from (a) mouse 3 expressing GCLink and (b) mouse 4 co-expressing eGFP and mCherry, with left image: MRI; central image: reconstructed MAP lifetime distribution (τ); right image: merged. Panel **(c)** shows fluorescence lifetime histograms of tomographic reconstructions from mice 3 and 4. These values are extracted from a volume defined by the top 30% of the calculated quantum yield distribution.

Table 1 summarizes the eGFP reconstructed lifetimes and quantum yields from *in vivo* time-gated measurements of five mice and calculated from a volume defined by the top 30% of the reconstructed quantum yield distribution.

Averaging over the data from all five animals, the mean eGFP lifetime was 1.335 ± 0.234 ns (n = 3) for mice expressing GCLink and 2.238 ± 0.164 ns for the control mice (n = 2). The donor eGFP of the GCLink FRET construct thus exhibits a consistently lower mean fluorescence lifetime compared to the free eGFP co-expressed with mCherry, showing that the lifetime reduction is specific to the GCLink FRET construct and is not due to intermolecular

#146182 - $15.00 USD Received 18 Apr 2011; revised 6 Jun 2011; accepted 10 Jun 2011; published 10 Jun 2011

**Table 1. Mean eGFP fluorescence lifetimes and quantum yields**

| Mouse # | Average Lifetime (ns) | SD | Average Quantum Yield | SD |
|---|---|---|---|---|
| 1 GCLink | 1.308 | 0.223 | 0.058 | 0.005 |
| 3 GCLink | 1.116 | 0.270 | 0.068 | 0.006 |
| 5 GCLink | 1.582 | 0.159 | 0.068 | 0.006 |
| 2 eGFP + mCherry | 2.354 | 0.245 | 0.058 | 0.005 |
| 4 eGFP + mCherry | 2.122 | 0.341 | 0.081 | 0.007 |

**Table 2. Time-resolved fluorescence spectroscopy of cytosol preparations of eGFP, GCLink and eGFP + mCherry**

| | $p_1$ | $\tau_1$ (ns) | $p_2$ | $\tau_2$ (ns) | $\chi 2$ | $\bar{\tau}$ (ns) |
|---|---|---|---|---|---|---|
| eGFP | 0.13 | 1.46 | 0.87 | 2.71 | 1.169 | 2.61 |
| GCLink | 0.40 | 0.80 | 0.60 | 2.42 | 1.289 | 2.13 |
| eGFP + mCherry | 0.11 | 1.41 | 0.89 | 2.69 | 1.051 | 2.61 |

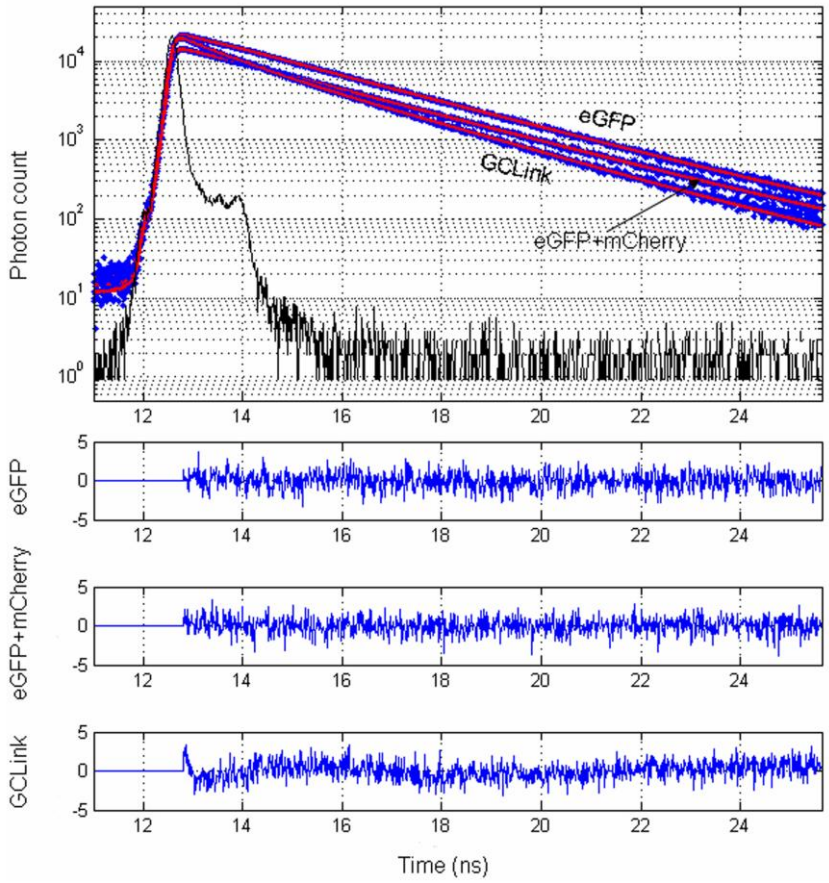


Fig. 3. Time-resolved fluorescence spectroscopy of cytosol preparations of eGFP, GCLink and eGFP + mCherry. The experimental data are displayed in blue, the fitting model in red and the Instrument Response Function (IRF) is displayed in black. At the bottom of the figure the residuals of the fits are shown.

FRET or to other factors associated with the local fluorophore environment. This reduction of eGFP donor lifetime due to FRET correlates with cuvette measurements of the same fluorophores in solution; see Table 2 and Fig. 3.

#146182 - $15.00 USD Received 18 Apr 2011; revised 6 Jun 2011; accepted 10 Jun 2011; published 10 Jun 2011

We note that the absolute lifetime values reconstructed from *in vivo* mouse data (as presented in Table 1) do not match the values from cuvette measurements (2.61 ns and 2.13 ns for the control and FRET constructs respectively). This is mainly due to the limitations of tomographic reconstruction of diffuse fluorescence signals (see Methods) although some variation may also be due to the properties of the fluorescent proteins. In particular, the variation in the lifetime of eGFP within the FRET construct may be due to partial maturation of the mCherry acceptor [17]. The essential point, however, is that FRET can be detected *in vivo* via a decrease in the absolute values of the tomographically reconstructed donor fluorescence lifetime and this can provide a usable readout to localize sites of protein-protein interactions or FRET biosensors. We note that tissue autofluorescence could also lead to incorrect reconstruction of fluorescence lifetime and quantum yields but we believe that this was not a significant issue for this experiment. To confirm this we compared the signals from mouse legs with and without the fluorescence proteins expressed. The autofluorescence signal was approximately 200x lower than the signal from eGFP in our detection window of 530 ± 20 nm.

In principle, FLIM is not required to map FRET since it can be read out via changes in quantum efficiency, which could be approximated by the reconstructed quantum yield. In practice, however, it is often not possible to reconstruct sufficiently quantitative data from steady-state fluorescence intensity measurements. Even for reconstructions from time-resolved data, such as we present here, the quantum yield is a less reliable indicator of FRET than the fluorescence lifetime because it can be modified by absorption of the fluorescence by the sample and by background absorption of the excitation radiation. This is borne out by Table 1. Nevertheless, it provides a useful indication of the fluorophore distribution and this was used to identify the voxels over which the mean fluorescence lifetimes were calculated. Figure 4 shows reconstructed quantum yield distributions for the two samples shown in Fig. 2.

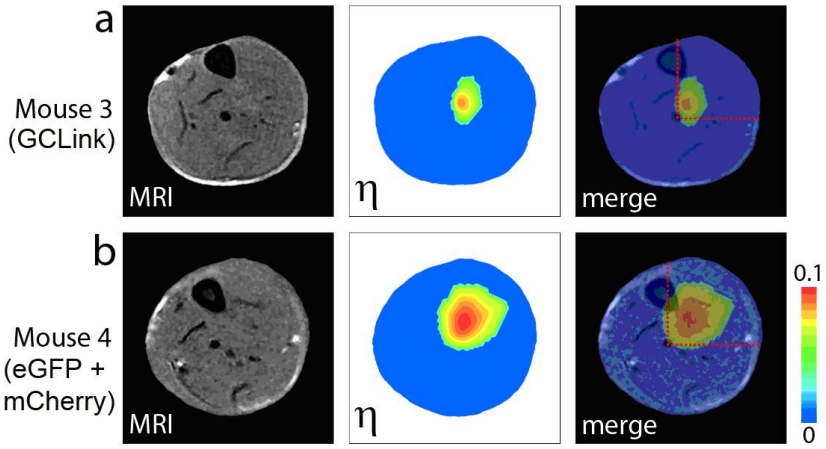


Fig. 4. Tomographic reconstructions of quantum yield distributions from *in vivo* FLIM of hind leg muscles. Leg cross sections expressing GCLink (a) and co-expressing eGFP and mCherry (b). Left side panel: MRI; central panel: reconstructed MAP quantum yield distribution (η); right panel: merged.

The localization of the reconstructed fluorescence distributions in the anterior lateral quadrant of the leg was verified by magnetic resonance imaging (MRI) acquired *post mortem* at the end of the *in vivo* optical experiments. Figures 2 and 4, panels (a) and (b), show the co-aligned MRI and reconstructed optical data separately and overlaid. In 3/5 cases the peak of the reconstructed signal distribution is located within the expected quadrant of the leg and in a fourth case the detected signals were just outside this region. We note that an apparent discrepancy in reconstructed fluorophore localization may reflect the actual distribution of the expressed fluorescence protein. To confirm the colocalization of eGFP and mCherry in the

#146182 - $15.00 USD Received 18 Apr 2011; revised 6 Jun 2011; accepted 10 Jun 2011; published 10 Jun 2011

GCLink and control transfected mice, sections of TA muscles were analyzed by confocal fluorescence microscopy. Figure 5, panel (a), shows that the fluorescence signals appear in the upper right leg quadrant, where the TA resides. The eGFP and mCherry fluorescence signals were observed to be overlaid as expected in both a GCLink transfected mouse (Fig. 5, panel b) as well as in a control mouse (panel c), confirming the validity of the control.

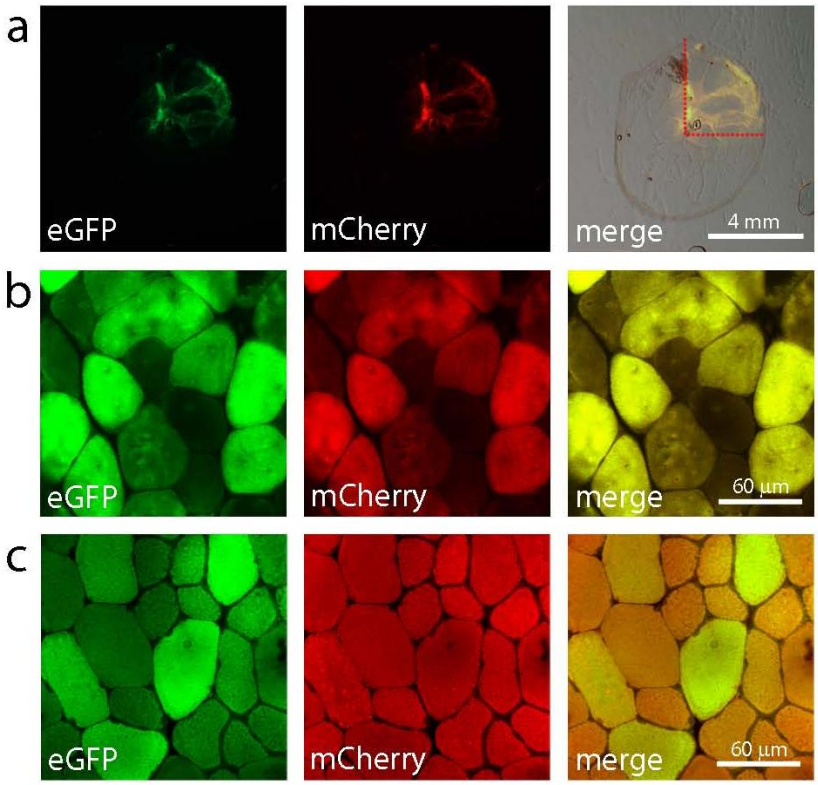


Fig. 5. Co-location of transfected fluorophores. Panel (a**)** shows fluorescence microscope images of a whole leg section of a mouse transfected with GCLink with left image eGFP signal; central image: mCherry signal; right image: combined bright field and fluorescent images with overlay of two fluorescent signals in yellow. Panels (b**)** and (c**)** show confocal sections of TA muscles from mice transfected either with GCLink (b) or eGFP and mCherry (c) respectively with left image: eGFP signal; central image: mCherry signal; right image: overlaid.

## 4. Conclusions

To our knowledge this is the first report of *in vivo* tomographic fluorescence lifetime mapping of a FRET probe genetically expressed in a small animal. It provides a key advance towards the practical application of FLIM FRET to read out molecular interactions and biosensors *in vivo*. We note that the precision of fluorophore localization can be compromised by the absorption and scattering of excitation and fluorescence radiation and by the background autofluorescence of the biological tissue. The impact of absorption and scattering could be mitigated by engineering FRET probes with donor-acceptor combinations utilizing fluorophores that are both excited and emit at longer wavelengths, such as red and near infrared fluorescent proteins. A recent study has shown the advantage of red-shifted fluorescent protein for *in vivo* tomographic imaging and demonstrated that, while autofluorescence is still a significant issue, it can be accounted for in the tomographic reconstruction to provide improved sensitivity, spatial localization and reduced image

#146182 - $15.00 USD Received 18 Apr 2011; revised 6 Jun 2011; accepted 10 Jun 2011; published 10 Jun 2011

acquisition times [18]. The total acquisition time could be decreased further by automating the image acquisition process and investigating the trade-off between the number of time gates and the number of projection angles. We note that the time-resolved image data could also be acquired in the frequency domain using a sinusoidally modulated wide-field detector and we expect that both time and frequency domain approaches could be optimized to reach a similar level of performance. With appropriately engineered fluorophores, the plethora of existing genetically expressed intracellular FRET biosensors could be exploited, reading out intracellular messengers such as calcium, IP3, GTP and PIP2, in addition to a vast array of intermolecular FRET readouts of protein binding [19,20]. In the current study we imaged the hind leg muscle because it provides a convenient target for *in vivo* plasmid transfection that allowed us to efficiently express our fluorescent probes in the same cells that make the organ, the myotubes, without alteration of its anatomical architecture. The creation of genetically modified mice expressing FRET probes would permit imaging in almost any anatomical location and would facilitate longitudinal studies in a variety of research fields. Examples of such studies include: tracking tumor growth, progression and metastasis, xenograft rejection, reperfusion toxicity in brain and heart ischaemic models as well as assessing the effectiveness of pharmacological intervention.

**Acknowledgments**

This research was supported by a Wellcome Trust grant (086114). The plasmid coding for GCLink is a generous gift from Matilda Katan and Tom Bunney (ICR, London UK). We acknowledge the Biological Imaging Centre (BIC) of MRC, CSC for the MRI facility. P. M. W. French is recipient of a Wolfson Research Merit Award from the Royal Society.

#146182 - $15.00 USD Received 18 Apr 2011; revised 6 Jun 2011; accepted 10 Jun 2011; published 10 Jun 2011